Measuring self-reflectivity of a water surface with high intensity femtosecond laser pulses

June 17, 2015

Michiel Bruinewoud

Supervisors:
M. Scholten, BSc
dr. D van Oosten

Abstract

For this research we attempted to measure the reflectivity of short high intensity laser pulses on a water surface. Due to the high intensity, part of the surface is converted to a plasma causing a shift in reflectivity. However,while building the setup we encountered multiple technical difficulties. Due to these difficulties we never reached high intensities. We did manage to measure the unchanged reflectivity of the water surface, which can be used as a calibration for further measurements of the self-reflectivity. This reflectivity turned out to be 0.0201 ± 0.0001.

Contents

1 Introduction

In the field of nanophotonics, interactions between matter and light are studied on a microscopic scale. In the process of laser ablation, laser pulses with a very high intensity are used to remove material from the sample. This technique is used to create nanostructures[1], to cut away tissue in medicine and in manufacturing of processors[2]. When the material absorbs a laser pulse of high enough intensity, part of the material is converted to plasma and removed from a sample. This happens on a very short timescale so other processes such as thermal diffusion are neglectable.

In this research very short laser pulses ($\sim$100 fs) were shot at a water-air interface. Comparable research has only been conducted on the nanosecond scale[3, 4]. Water is an interesting material when it comes to its optical properties. Water is transparent to visible light, and its optical properties are much like glass. The refractive index of normal glass is n=1.45. The refractive index of water at room temperature is 1.33. This indicates that glass and water display similar behaviour when supporting a electromagnetic wave. The absorption spectra of both materials also display many similarities. Furthermore, glass is an amorphous solid, which means that glass does not display a crystalline structure. Water does not display a crystalline structure either, because it is a liquid. Femtosecond laser ablation has been done numerous times on glass samples, but never on liquid water samples. Interesting is what happens to the pulse when the material is converted to a plasma. Due to the different electrical properties of this plasma, the pulse is reflected in a different way. This so called self-reflectivity is what was measured in this research.

This thesis describes the work I have done in the last semester: Building the experimental setup and measuring the self-reflectivity of water. During the building of the setup we encountered several technical difficulties, delaying the actual measuring. The theory to understand the process of laser ablation, and the solutions to the technical difficulties are discussed in the next sections. In section 4 measured data is discussed, and possible solutions for the technical difficulties are discussed.

2 Theory

2.1 Laser theory

Some understanding of lasers and their characteristics is needed to understand the rest of the theory. In this first section, some important aspects of lasers are explained.

2.1.1 Laser

A laser is a device that produces a coherent beam of light using optical amplification. The process that forms the basis of this amplification is called stimulated emission. In stimulated emission, a photon of a specific energy can cause an excited atom to decay to a lower energy level, under the emission of another photon. Note that this exciting photon has to be the same energy as the emitted photon. In lasers, the part responsible for the stimulated emission is called the gain medium which is often a crystal (in this case a Ti:sapphire crystal). An energy source is needed to excite the atoms of this medium. This is often done by another laser, which is called the pump laser. The amplified light does not leave the laser immediately. Mirrors are placed on both sides of the gain medium. One of the mirror has a very high reflection (the high reflector) and the other (the output coupler) allows a small fraction to be transmitted. The space between the two mirrors is called the cavity. Now, photons coming from the crystal are sent back through the crystal many times before they leave the laser. Every time they pass through the gain medium, they stimulate emission . The alignment of these mirrors is the cause of the precise direction of the laser beam. This process is clarified in Figure 1.

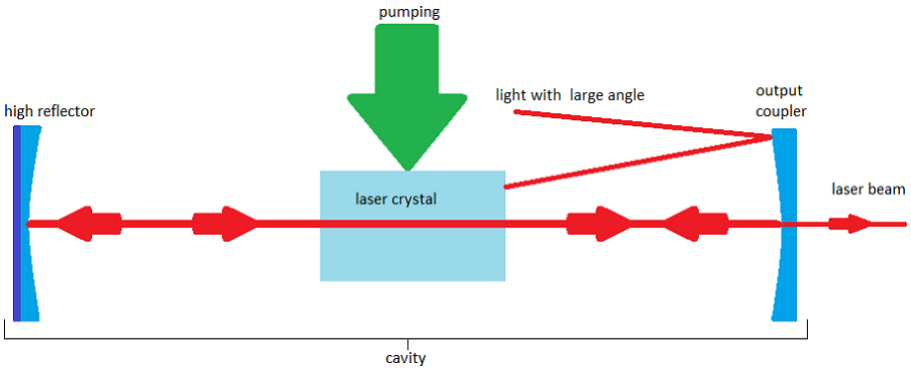

Figure 1: The principle of a laser. Light bounces back and forth in the cavity until it is transmitted by the output coupler. Light that is emitted from the crystal under an angle that is too large is lost because it is not reflected back in the cavity. This causes the beam to be highly directed.

2.1.2 Gaussian beam

Many lasers, and also the laser used in this research, produce light in the form of a Gaussian beam. A Gaussian beam is a transverse electromagnetic mode (TEM) which means that the electric field and the magnetic field components of the electromagnetic wave are perpendicular to its direction of propagation. The distribution of the electric field is radially symmetrical and so is the intensity. For the electric field we have, when neglecting the phase

$$E(r) = E_0 \exp\left(-\frac{r^2}{\omega_0^2}\right) \tag{1}$$

Where r is the radial distance from the center of the beam , ω_0 is the radius where the amplitude of the electric field is 1/e of the value in the center and $E_0$is the electric field in the center.
The intensity of the beam (W/m^2) also has a Gaussian distribution

$$I_s = \eta E_0^2 \exp\left(-\frac{2r^2}{\omega_0^2}\right) \tag{2}$$

Where η is the impedance of the medium ($\sqrt{\frac{\mu}{\epsilon}}$). An important parameter, ω_0, emerges in both equations. This parameter is known as the beam waist. The waist has a minimum value at some point , the focus of the beam, and is not a constant. For the waist at distance z from the focus we have

$$\omega(z) = \omega_0 \sqrt{1 + \left(\frac{z}{z_R}\right)^2} \tag{3}$$

Where $z_R$is the so-called Rayleigh range. The Rayleigh range is defined as

$$z_R = \frac{\pi \omega_0^2}{\lambda} \tag{4}$$

With λ the wavelength of the light. The Rayleigh range is important because it gives insight in what range the beam stays in focus. This parameter will emerge again later on.

2.1.3 Fluence

Laser fluence is a measure of the amount of energy per area delivered by the laser. It is defined as the amount of energy in one laser pulse (J) divided by the area of the focal spot (cm^2). The amount of energy in one pulse is defined as the peak power (W) multiplied by the duration of a pulse (s). The area we pick is a circle with a radius of the 1/e-width of the beam. Here, the intensity has fallen to a fraction of 1/e of the original. To have any effect on the sample, the fluence has to be high enough to turn part of it into plasma. The lowest fluence at which ablation occurs is called the ablation threshold.

2.2 Mode-locking

When operated normally, a laser works in continuous-wave mode (CW), which means that light is always coming out of the output coupler at the same intensity. To get a fluence high enough to exceed ablation threshold the laser has to be operated in a different way. CW does not deliver the peak intensity needed for ablation. Therefore, the technique of mode-locking is introduced. When a laser is mode-locked, a short pulse bounces between the mirrors until it is let out. The time between it takes for a pulse to make a round trip depends on the distance between the mirrors. The time is fixed for a pulse, and so a mechanical shutter can be used to let the pulse out of the cavity. This way of mode-locking (active mode-locking) has two major problems. . In the laser we used the time it takes a pulse to travel from one end of the cavity to the other is 19 ns, resulting in a frequency of 54.3 MHz. This frequency is very hard to achieve for optical shutters, and even harder for mechanical shutters. The second problem is that there will still be a CW-component in the cavity. When utilizing shutters, a part of this CW-component is let through. Another type of mode-locking is more suitable for this kind of frequency: passive mode-locking. When mode-locking passively, another process is utilized. In many lasers this is done by exploiting the optical Kerr effect. This is a process where the electric field of the electromagnetic wave causes a nonlinear effect in the refractive index of some medium, the Kerr medium. When the intensity is high enough, the Kerr medium works as a lens, but only for the high intensity light (the pulse). The CW-component that is still present in the cavity is left unaffected by the Kerr medium. When the Kerr lens is shaped correctly, it will focus the pulsed light, and defocus the CW-light. When combined with a adjustable slit, one can filter out a part of the CW-component while letting through the pulsed light. The rest of the CW-component will still be present, but per round trip more of it gets absorbed than amplified. This causes the CW-component to die out. This principle is illustrated in Figure 2

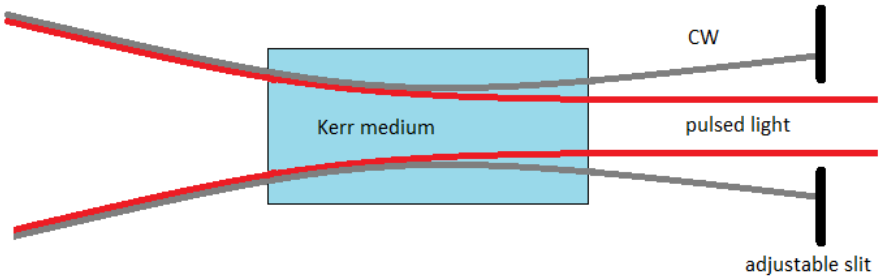

Figure 2: Passive mode-locking with a Kerr medium. The pulsed light is focused by the Kerr medium while the CW-component is defocused. The adjustable slit cuts away the CW-component.

2.3 Cavity dumping

To gain control over which pulses leave the cavity, a cavity dumper can be placed in the cavity of a laser. A cavity dumper often uses an acousto-optic deflector (AOD) to select pulses. An AOD utilizes the acousto-optic effect to deflect pulses out of the cavity. In the acousto-optic effect, the permittivity ϵ of the medium changes due to an acoustic wave in the medium. Changing the permittivity means changing the refractive index. The change in refractive index (and thus the diffraction angle) depends on the frequency of the acoustic wave in the medium. An OAD usually uses one frequency which is in the Bragg regime

$$\sin\theta_b = \frac{\lambda}{2\Lambda} \tag{5}$$

Where θ_b is the incident (Bragg) angle of the beam, λ is the wavelength of the beam and Λ is the wavelength of the acoustic wave in the medium. In this regime, all diffracted waves are annihilated by destructive interference, except for the first order. Many OADs use radio-frequency (RF) acoustic waves. When turning this RF signal on and off quickly enough, a cavity dumper can select which ratio (division ratio) of the pulses is deflected. These devices do not reach 100% efficiency i.e. the pulses are not deflected completely. Most efficiencies lay in the range of 65-90%. However, some mechanism (reflection on the Bragg crystal) causes pulses that are not selected to leak out of the laser.The efficiency of the cavity dumper gives rise to an important aspect of these devices: the pulse contrast ratio. This ratio shows how high the intensity of the selected pulse is in comparison to the leaking pulses. High pulse contrast means a highly efficient cavity dumper. Typical contrast ratio's range from 300:1 to >500:1. To increase the efficiency, a technique called double-pass cavity dumping is applied. This technique can increase pulse contrast by creating constructive interference between the dumped pulse and its remainder. This process is clarified in Figure 3

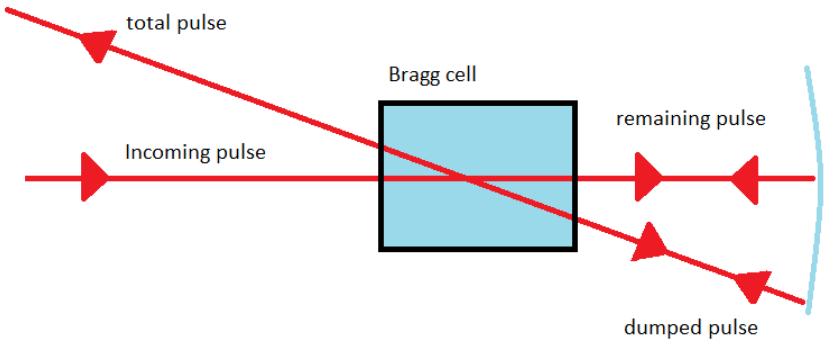

Figure 3: Double-pass cavity dumping. The total pulse can be enhanced by creating constructive interference between the dumped pulse and the remaining pulse, resulting in a higher pulse energy and a better pulse contrast ratio.

Constructive interference can be achieved by fine-tuning the frequency and the phase of the RF signal in the Bragg cell. In the Bragg cell, the pulse will shift in frequency that depends on the frequency of the RF signal ν. When we assume that the envelope of the pulse is given by $E(t) = E_0 \cos(\omega t)$, the expressions for the dumped pulse E_d and the remaining pulse E_r are

$$E_d = \sqrt{\eta} E_0 \cos(\omega t + \nu t + \Phi) \tag{6}$$

$$E_r = \sqrt{1-\eta} E_0 \cos(\omega t + \nu t + \Phi) \tag{7}$$

Where η is efficiency, ν the frequency of the RF signal and Φ the phase of the RF signal. The total pulse is the sum of the dumped and remaining pulse. When changing Φ one can achieve constructive interference, increasing the total efficiency of the cavity dumper. Using a cavity dumper will increase pulse intensity. A laser with a cavity dumper uses two high reflectors instead of one and a output coupler. This causes more of the light to make a round trip (passing through the gain medium twice) so the pulses are more intense. A laser with an output coupler typically transmits 20% of a pulse from the cavity, while a laser with a cavity dumper can reach an efficiency of 60%.

2.4 Electromagnetic waves in a medium

Light is an electromagnetic wave,so it does not only have an electric field, but also a magnetic field. Both of these field interact with the medium the wave is propagating in. When traveling from one medium to another the direction of the beam changes, it refracts. Maxwell's equations describe the behaviour of light in a medium. These equations look like this

$$\nabla \times \vec{E} = -\frac{\partial \vec{B}}{\partial t}, \tag{8}$$

$$\nabla \times \vec{H} = \frac{\partial \vec{D}}{\partial t} + \vec{j}, \tag{9}$$

$$\nabla \cdot \vec{B} = 0. \tag{10}$$

$$\nabla \cdot \vec{D} = \rho. \tag{11}$$

In these equations $\vec{E}$ is the electric field, $\vec{B}$ the magnetic induction, $\vec{H}$ the magnetic field, $\vec{D}$ the electric displacement, j the free charge current density and ρ is the free charge density. All of these variables depend on position and time. Some of these parameters can be replaced by other equations when the wave is traveling through a material. These equations are

$$\vec{D} = \epsilon_0 \epsilon \vec{E}, \tag{12}$$

$$\vec{B} = \mu_0 \mu \vec{H}, \tag{13}$$

$$\vec{j} = \sigma \vec{E}. \tag{14}$$

With ϵ the dielectric constant, μ the magnetic permeability and σ the specific conductivity. These three parameters are specific for the medium. The permittivity of free space, ϵ_0 , has a value of 8.854×10^{-12} F/m and μ_0, the permeability of free space, has a value of $4\pi \times 10^{-7}\mathrm{N/A}^2$. Most materials, and in our case water, are non-magnetic so $\mu = 1$. The so-called constitutive relations (relations between physical quantities in a specific material) for electromagnetic waves in a medium are

$$\vec{D} = \epsilon_0 \vec{E} + \vec{P}, \tag{15}$$

$$\vec{H} = \frac{\vec{B}}{\mu_0} - \vec{M}. \tag{16}$$

P and M are, when the fields are weak enough:

$$\vec{P} = \epsilon_0 \chi \vec{E}, \tag{17}$$

$$\vec{M} = \chi_m \vec{H}. \tag{18}$$

Here χ is the dimensionless static susceptibility and $x_m$is the dimensionless magnetic susceptibility. When we put Eqs. 9, 10 and 12-14 together, we end up with a simple result.

$$\epsilon = 1 + \chi, \tag{19}$$

$$\mu = 1 + \chi_m. \tag{20}$$

When working with water this gets even more simplified. At optical frequencies, $\mu = 1$. Water is non-magnetic (or actually it is diamagnetic) so $\chi_m = 0$. Lastly, the refractive index of the medium can be calculated.

$$n = \sqrt{\epsilon\mu}. \tag{21}$$

But since we have $\mu = 1$, we end up with:

$$n = \sqrt{\epsilon}. \tag{22}$$

So the refractive index of a non magnetic material only depends on its dielectric constant. But the dielectric constant is wrongfully called a constant. It actually depends on the frequency of the electromagnetic wave in the material. Furthermore, when a material gets hit by a pulse with enough energy, part of it converts to plasma. This changes the value of ϵ, thus changes the reflectivity. The relations between the refractive index and the reflectivity are the so-called Fresnel equations

$$R_\perp = \left| \frac{n_1 \cos\theta_i - n_2 \cos\theta_t}{n_1 \cos\theta_i + n_2 \cos\theta_t} \right|^2, \tag{23}$$

$$R_\parallel = \left| \frac{n_1 \cos\theta_t - n_2 \cos\theta_i}{n_1 \cos\theta_t + n_2 \cos\theta_i} \right|^2 \tag{24}$$

Where the subscripts $\perp$ and $\parallel$ indicate the direction of the polarization of the light ,θ_i is the incident angle, and θ_t is the angle of transmission. In our case $\theta_i = \theta_{t=}0$ so Eqs. 23 and 24 become

$$(\frac{n_1 - n_2}{n_1 + n_2})^2 \tag{25}$$

When putting in the refractive indices of air and water, we arrive at an unperturbed reflectivity of 0.0201.

2.5 Laser ablation

When fluence is high enough, the incident light can ionize the material. The binding energy of a electron in the valence band is around one electron volt. Because these electrons are positioned very close ($\sim 10^{-11} m$) to their atoms, this binding energy corresponds with a strong binding field. Force scales with binding energy over distance, so this binding field has a strength of around 2×10^{10} V/m. For the intensity of an electric field we have:

$$I = \frac{cn\epsilon_0 |\vec{E}|^2}{2} \tag{26}$$

With c the speed of light. If we put in the relevant numerical values we arrive at an intensity of $\sim 2 \times 10^{13}$ W/cm^2. If we assume that a single pulse from the

laser has a duration of 100 fs and the spot size is 1 μm^2 we need a fluence of 2 J/cm^2, meaning that the laser needs to produce an energy of 20 nJ per pulse.

2.5.1 Drude model

As said in section 2.3, the dielectric constant ϵ is not a constant but a function of wavelength. A plasma has a different dielectric function than a solid or liquid. This change in the dielectric function is what causes non-linear behaviour in the reflection of a pulse. In this section the dielectric function of a plasma (also called a free electron gas) is described.
The Drude model describes how free electrons move in a solid. The electrons bounce between the atoms in the crystal. In this research we are working with liquid water so the atoms will not be ordered neatly on a crystal and will be moving, in contrary to a solid. However, the duration of a laser pulse is small enough to assume that the atoms of the water are stationary during the irradiation. So the Drude model is used to describe the behaviour of the sample. Some of the equations from section 2.3 change when considering the Drude model. Now we have:

$$\vec{j} = \left(\frac{Nq^2\tau}{m}\right)\vec{E} \tag{27}$$

Where j is the free charge current density, N the number density of electrons, q the charge of an electron, τ the mean free time between collisions and m the mass of an electron. We assume free moving electrons. The only force working on them is the Lorentz force from an electric field. So the equation of motion for an electron is

$$\frac{\partial\vec{p}}{dt} + \frac{\vec{p}}{\tau} = -e\vec{E} \tag{28}$$

Where p is the momentum of the electron, and e the charge of an electron. We know that the electric field is oscillating because it is the field of the electromagnetic wave. So Eq 28 becomes

$$\frac{\partial\vec{p}}{dt} + \frac{\vec{p}}{\tau} = -e\vec{E}\exp(-i\omega t) \tag{29}$$

Now we want to solve this equation of motion of an electron in an oscillating electric field. The solution will have the form of $A\exp(-i\omega t)$. When plugging this trial solution into Eq 27 we arrive at

$$\vec{p}(t) = \frac{-e\vec{E}\exp(-i\omega t)}{1/\tau - i\omega} \tag{30}$$

When we combine this equation with Eq 22 and Eq 12 we arrive at the conductivity. The conductivity can be used to find an expression for the permittivity. The electric current density equals the sum of the free electrons per unit volume

$$\vec{J} = \frac{-Ne\vec{p}}{m} \tag{31}$$

Combining this expression with Eq. 27 and 14 gives us, for the conductivity

$$\sigma(\omega) = \frac{Ne^2\tau}{m}\frac{1}{1-i\omega\tau} \tag{32}$$

We can use this expression in combination with

$$\epsilon(\omega) = 1 + \frac{i\sigma}{\epsilon_0\omega} \tag{33}$$

to arrive at the permittivity

$$\epsilon(\omega) = 1 - \left(\frac{\omega_p}{\omega}\right)^2 \frac{1}{1+\frac{i}{\omega\tau}} \tag{34}$$

Where we introduced the so-called plasma frequency, $\omega_p = \sqrt{\frac{ne^2}{\epsilon_0 m}}$. Now we can find an expression for the total permittivity and thus for the refractive index. The total permittivity is just the normal permittivity of water plus the change from the Drude response:

$$\epsilon_{tot} = \epsilon_w - \left(\frac{\omega_p}{\omega}\right)^2 \frac{1}{1+\frac{i}{\omega\tau}} \tag{35}$$

And finally we arrive at the refractive index n:

$$n = \sqrt{\epsilon_w - \left(\frac{\omega_p}{\omega}\right)^2 \frac{1}{1+\frac{i}{\omega\tau}}} \tag{36}$$

When a medium has free carriers (electrons) the effective refractive index changes and causes the reflectivity to change. Measuring the change of this reflectivity is the goal of this research. There has to be a physical process that causes the amount of carriers to rise in the medium. This process is not known exactly, but most likely it is a combination of one-photon absorption (OPA) and two-photon absorption (TPA).

2.5.2 Two-photon absorption

To create the free carriers, the water has to absorb the the photons. The combination of OPA and TPA is responsible for the high concentration of free carriers. The laser intensity inside a material where OPA and TPA occurs is given by a differential equation in the form of:

$$\frac{\partial I}{\partial x} = -\alpha I - \beta I^2 \tag{37}$$

Where α is the OPA coefficient and β the TPA coefficient. This absorption creates the free carriers in the plasma. Taking the diffusion of the carriers into

account, the number density N of the free carriers can be expressed in terms of this diffusion and the absorption:

$$\frac{\partial N}{\partial t} + \nabla \cdot (-D\nabla N) = \frac{\alpha_0 I}{\hbar\omega} + \frac{\beta I}{2\hbar\omega} \tag{38}$$

Where D is the diffusivity coefficient and $\hbar\omega$ is the photon energy of the incoming beam. In our case, where the Drude response plays a big part in the top layer of the material, Eq 33 takes the form of:

$$\frac{\partial I}{\partial x} = -(\alpha_0 + \alpha_{drude})I - \beta I^2. \tag{39}$$

Here $\alpha_0 = 2.29$ m^{-1} (at 20 °C, $\lambda = 800$ nm) and β is the TPA coefficient. The intensity depends on the reflectivity of the surface: $I = (1-R)I_0$where R is the the surface reflectivity, and I_0 is the incoming laser intensity. The absorption changes due to the term α_{drude} once the carriers are created by the OPA and TPA. α_{drude} is given by:

$$\alpha_{drude} = \frac{4\pi\kappa}{\lambda}, \tag{40}$$

Where κ is the imaginary part of the complex refractive index n, given by Eq. 32.

3 Setup

In this section the setup that was built and used during the measurements is described in detail. Figure 4 gives an overview of the experimental setup.

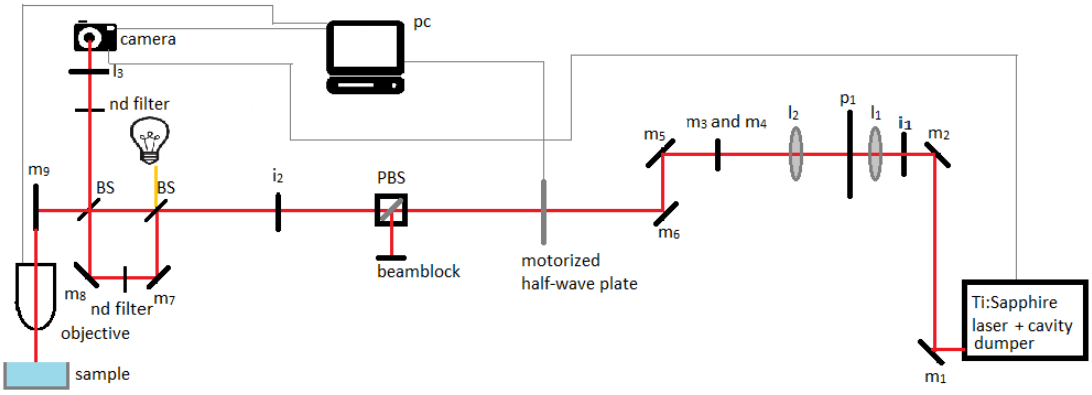

Figure 4: The setup as seen from above. The function of every part is described below.

- **Laser with cavity dumper:** the Coherent Mira 900 Ti:Sapphire laser, operating at 54Mhz at 800 nm, used for the experiment combined with the A.P.E. PulseSwitch cavity dumper, responsible for selecting the pulse that is fired on the sample. The laser uses passive mode-locking, and the cavity dumper should give a pulse contrast ratio of >500:1
- **m_1- m_9:** Mirrors are used to redirect the beam and for alignment. All mirrors and lenses are coated with the Thorlabs B-coating, which has optimal behaviour for light at 800 nm.
- **i_1:** the first iris on the beam path, used to spatially filter some of the beam because some of the light was unwanted (more on this later).
- **l_1:** the first lens of the telescope with f=5 cm.
- **p_1:** a pinhole mounted on a micrometer stage is used to further cut off the background light leaking from the laser.
- **l_2:** the second lens of the telescope system. This lens has a focal length of f=12.5 cm. The ratio of the focal lengths of the two lenses determines the spotsize. The second lens has to be in the right position to make a parallel beam. Hence it is placed on a micrometer stage.
- **half-wave plate:** this device is used to control the polarization of the laser light. Rotating it changes the polarization.

- **PBS:** this cube splits the beam depending on its polarization. At 90 degrees polarization angle all of the beam is directed away from the sample, and at 0 degrees polarization angle all of the light is transmitted. In combination with the half-wave plate this cube works as power control.
- **beamblock:** used to block the beam coming from the beamsplitter cube. This light is not needed.
- $\mathbf{i_2}$**:** the second iris on the beam path. This iris is used for alignment purposes and for spatial filtering.
- **BS:** these pellicle beamsplitters split the beam into two paths. The first one is used to split the beam into a path to the sample and one to the camera. The beam going to m_7 is the reference-beam. The second one is used to direct the beam reflected by the sample into the camera. The splitters have a transmission/reflection ratio of 55/45
- **objective :** the objective is used to create a small focus on the sample, which is located under it. The objective is movable in the vertical direction, making it possible to obtain a focus on samples of different heights.
- **sample**: an aluminium container with a layer of water. the pulse sent to the sample is reflected on the surface back to the camera.
- **ND filter:** these neutral density filters are used to attune the light coming into the camera.
- $\mathbf{l_3}$: a lens placed in front of the camera, its function is to focus the incoming image on the camera.
- **lamp:** this lamp is used to see if the sample is in focus. Small pecs of dust and other features on the sample are visible on the camera when this is the case. The lamp is a combination of 3 LEDs and a lens.
- **Camera:** the Andor Zyla 5.5 camera that is responsible for collecting data. The camera is connected to the PC and to the external trigger input of the cavity dumper. The camera has a bit-depth of 16, meaning it will give a pixel value of 0 when no light hits the pixel, and a value of 65535 when saturated.
- **PC**: the half-wave plate, the stage on which the objective has been mounted and the camera are connected to and controlled by the PC.

The objective used is a high numerical aperture (NA) objective. NA is a measure for the angle of the light that the aperture accepts. A high NA objective has a much smaller working distance than a low NA objective because of the large angle of acceptance. This large angle is makes this objective very suitable for experiments where light is scattered. NA is defined as:

$$NA = n_i \sin(\theta) \tag{41}$$

Where n_i is the refractive index of the medium, and θ is the angle of the light with respect to the normal of the aperture. In Figure 5 a comparison between a low NA and high NA situation is made. Such high NA objective create foci that have a small width ($\sim \mu m$). Because of this, the depth of focus of these objectives is very small. In our case, the depth of focus is in the order of a micrometer. This means that moving the objective a micrometer up or down causes the sample to go out of focus. This is why the objective has been placed on a stage that is movable in increments of 0.01 μm. The objective works best when the beam entering it is parallel, so the beam needs to be in focus on the back focal plane of the objective. The NA of the objective we used is 0.8, so $\theta = 52.7$

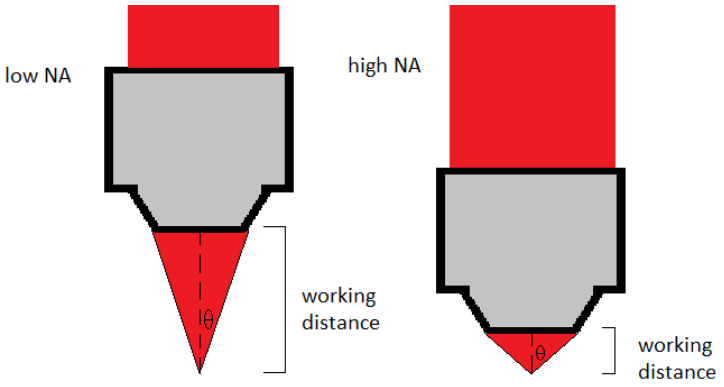

Figure 5: A comparison between low and high NA objectives. The small working distance and the large angle of acceptance makes this high NA objective very suitable for this experiment.

The software that controls the camera has options to select various trigger modes and to set exposure time. In our case, the shorter the exposure time, the better. We use rolling shutter mode, which means that all rows of sensors in the camera are exposed one after each other. When the last row of the camera is fired, the camera sends a signal to the output fire n. When all the rows are exposed, the camera sends a signal (fire all in Figure 6) to the aux output. Fire n or fire all can be used to trigger the laser. However, to take a reference shot of the background, we need to make a picture while not triggering the laser. This is why the output that is connected to the cavity dumper is put through a NAND gate. The NAND gate is also connected to the PC. When the software sends a signal to the NAND gate, the NAND gate gives no signal and a reference picture is taken. Figure 6 shows how all the signals relative to each other.

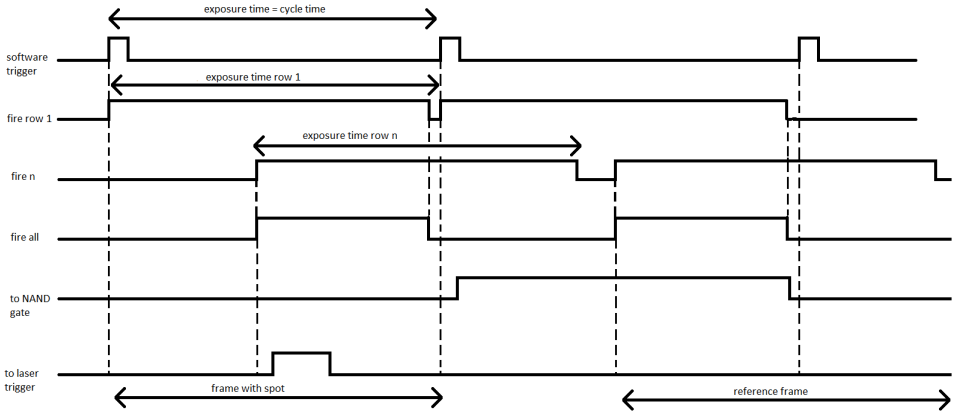

Figure 6: All the signals that come from the camera and the PC. The NAND gate controls whether the cavity dumper selects a pulse.

3.1 Optimizing spotsize

To get high enough fluence spotsize needs to minimized, or at least small enough so that fluence is above ablation threshold. To minimize spotsize, a telescope was built into the setup. The ratio of the focal lengths determines the magnification of the spot. When working with a parallel beam, constructing a telescope is simple. The distance between the lenses has to be equal to the sum of the focal lengths. However, the beam coming from our laser is slightly divergent, meaning that the position between the lenses does not equal the sum of the focal lengths. Varying the distance between the two lenses changes the convergence of the beam coming out of the telescope. This can be used to optimize spotsize. To determine which focal lengths have to be used, simulations were performed. In these simulations, two virtual lenses can be used to simulate the divergence of the beam. First, this divergence has to be measured. This is done by simply setting up a camera in the beam path. Different spotsizes were measured by varying the distance between the origin of the beam and the camera. The divergence of the beam was parameterized using these spotsizes. As can be seen in the top figure in Figure 7 two data point give a smaller beamwidth at a larger distance. Because it is impossible for a beam to have this kind of curvature without using lenses, we omitted these points from the calculation. To get a small spot on the sample that has enough fluence, there needs to be a focus at the back focal plane of the objective (at 2.6 m from the origin). This focus needs have roughly the same size as the back focal plane of the objective ($\sim$1.5 mm) to make it work optimally. Having a larger focus than the hole of the objective means cutting off parts of the beam. This will result in a beam that is not a Gaussian. Furthermore, cutting of parts of the beam means less intensity on the sample. Having a beam with a width that is much smaller than 1.5 mm would effectively decrease the NA of the objective, resulting in a bigger focus.

The top of the objective is on a fixed distance from the origin so the only two variables left are the focal lengths of the telescope lenses, and their positions. After running the simulation with different lens combinations, a combination of a f=12.5 cm and a f=5 cm would work best.

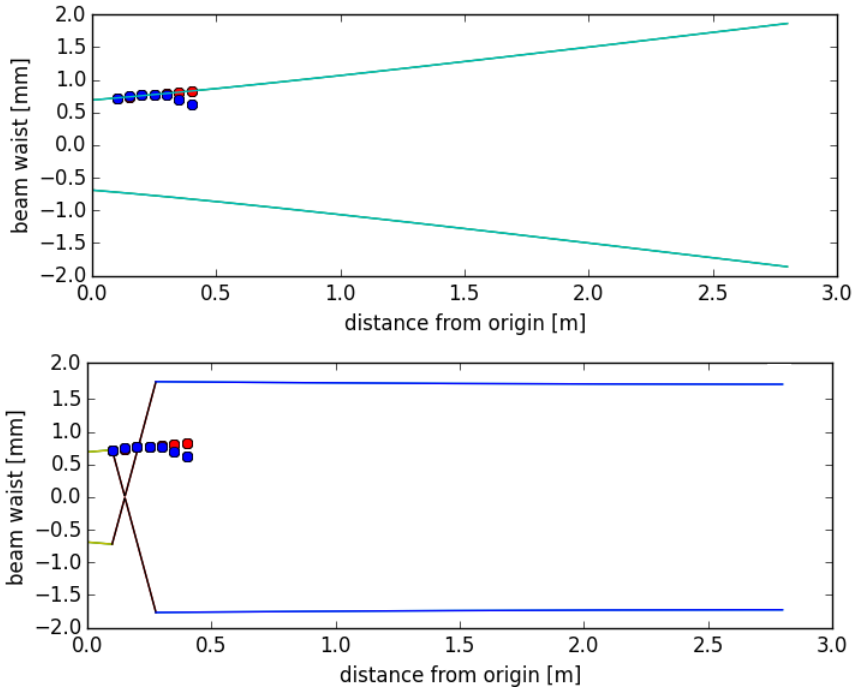

Figure 7: Simulations done to determine which combination of lenses would make a suitable combination for the telescope. The top figure displays the divergence of the beam and the measured beam waist. The bottom figure displays the beam as it is with the lenses we used.

3.2 Optimizing signal to background ratio

Unfortunately, the beam from the laser used in the setup is not a circular Gaussian as it should be, but it has more of a cigar shape. the cause of this is not known at the moment, because the laser system has only been installed recently. To get a spot small Gaussian on the sample, a more or less circular focus was needed on the back focal plane of the objective. The maximum pulse contrast ratio we obtained from the laser was 200:1, as opposed to the >500:1 specified in the data sheet of the laser. This means that 200 leakage pulses (pulses that are not selected by the cavity dumper) during one exposure time of the camera would result in the same intensity as the selected pulse. The camera would need to have an exposure time of ~3.5 microseconds or lower to work around this problem. The minimum exposure time of the camera is 10 microseconds, so this was not an option. Luckily, the leakage comes out of the laser at a slightly different angle than the selected pulse. This enabled us to apply spatial filtering to remove a large part of the leakage from the beam. To achieve this, multiple irises and a pinhole were placed along the beam path. As displayed by Figure 4, one of the irises was placed in front of the telescope, and one of the irises was placed near the polarizing beamsplitter. The pinhole was placed in the focus of the first lens of the telescope. By varying the size of the irises and the position of the pinhole, we could control how much of the beam was cut off. To see how much of a difference this spatial filtering made, a camera was placed on different positions on the beam path. The first position was in front of mirror 2, before any spatial filtering was applied. Two separate pictures were made at the same exposure time (140 ms), one with the cavity dumper selecting no pulses at all (thus showing leakage only) and one with the cavity dumper set to select pulses. Now the camera was moved to a position behind iris 2, so after the spacial filtering. Again, two pictures were taken, one of the leakage only and one with the pulse. These pictures were taken with the same exposure time as the first two pictures. All pictures were made at a division ratio set of 10, set on the cavity dumper. Figure 8 shows these pictures.

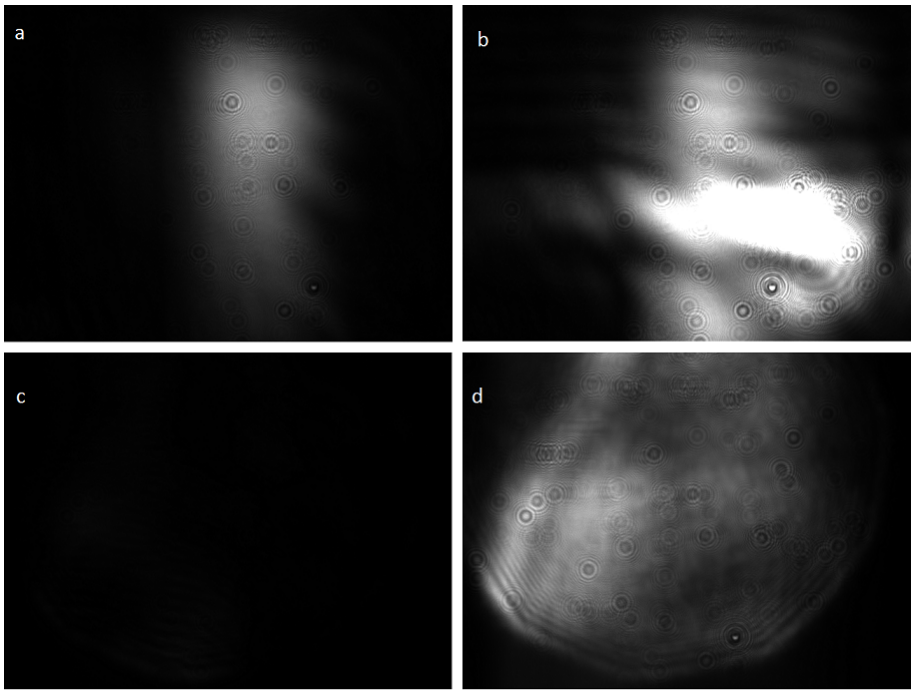

Figure 8: The pictures taken to see the effect of the spatial filtering. a) shows the leakage and b) shows the leakage and the pulse before any filtering was applied. c) shows the leakage after the spatial filtering, and d0 shows the beam after spatial filtering. The beam does not look much like a Gaussian, but the high NA objective can still make a Gaussian spot out of it.

To gain some insight in how much lower the leakage has become due to the filtering, a fifth picture was taken. This picture was made at a much higher exposure time (840 ms) than picture c) (140 ms). This exposure time was selected because it has the same amount of saturated pixels as d) and a) ($\sim$20) so a fair comparison could be made. This picture can be seen in Figure 9

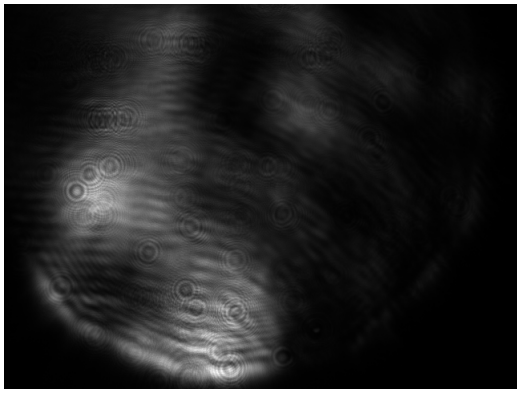

Figure 9: The leakage after filtering has been applied. The picture was taken with a exposure time of 840 ms. Leakage is still present, but the intensity is much lower. When compared to the leakage before the filtering, it has diminished by a factor 6.

3.3 Calibrating power

Before any measurements could be done, a calibration of the power was needed. A relation between the actual power and the total of the pixel values (pixel sum) on the camera is needed to process any data. The camera gives an output in the range of 0-65535 for each pixel, depending on how many photons hit this pixel. So a relation between the actual power and the pixel value was needed. To do so, a power meter was mounted under the objective. For every degree of the half-wave plate the camera took ten shots while the laser was firing pulses. After this, the camera took ten shots of the leakage. These values were subtracted to obtain the pixel sum of the actual spot. These ten values are then averaged. When the repetition rate of the laser and the exposure time of the camera is known, the value of power can be converted to energy. In figure 10 we see the energy plotted against the pixel sums. By applying a linear fit to the acquired data, we found the slope to be $2.20 \pm 0.02 \times 10^{-8} nJ/\text{ADU}$.

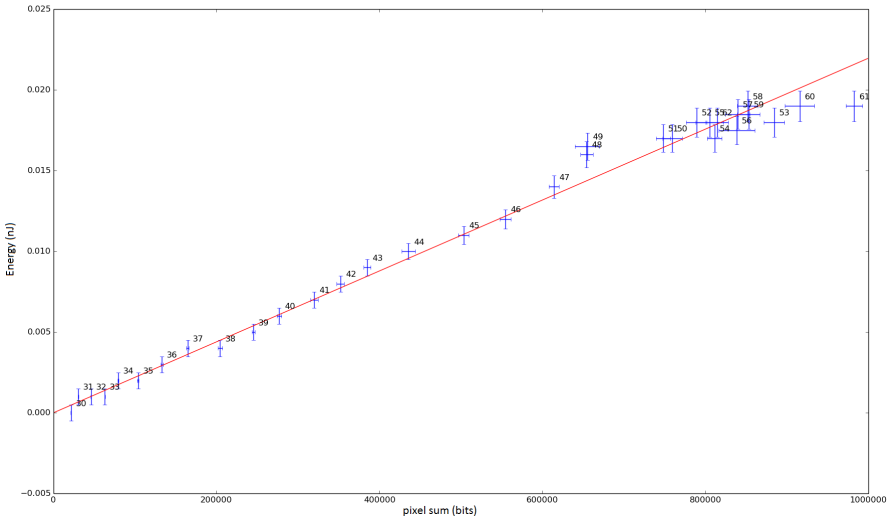

Figure 10: Power calibration. The energy plotted against the pixel sum on the camera. The numbers indicate the position of the half-wave plate. The red line indicates a linear fit with a slope of $2.20 \pm 0.02 \times 10^{-8} nJ/\text{ADU}$. This value will be used later on to process the data.

4 Results

To obtain these results, an aluminium container with a layer of ∼2 mm demineralised water was placed under the objective. The surface of the water needs to be in focus, so the lamp and camera were used to focus on the surface. To be sure that the surface was in focus instead of the bottom of the container, the container was moved by hand. This caused small waves to appear on the service of the water. These waves were visible on the screen, and the defocusing caused by the small depth of focus of the objective was clearly visible.
The measurements now described were done automatically. The computer controls the camera (and thus the laser) and the half-wave plate. The camera takes ten shots when triggering the laser, and one without sending a trigger signal. This last shot is subtracted as it is the background for the other ten shots. Then the half-wave plate is rotated with a step of 0.3 degrees and the process is repeated. Because the water is at room temperature, it slowly evaporates. The speed of this process was measured to be $\sim 40\mu m$ per hour. The small depth of focus of the objective means that this evaporization quickly causes defocusing of the surface. During the measuring the time was monitored. Any measurements taking longer than one minute had to be paused to refocus on the surface.
The data acquired by running this script is then loaded into another script. Here, the data set is cut into two separate data sets, one for the reflected beam and one for the reference beam. A pixel sum is applied to both beams, and a the data of the reflected beam is fitted to a Gaussian to determine spotsize. The fluence can be determined from the spotsize and the reference beam. Reflectivity is determined by the ratio of the pixel sums of the reflected beam and the reference beam. The selection criteria for the data were as follows: the Gaussian has a positive amplitude, the center of the Gaussian is in range of the camera, and the width in both directions ranges from 1 to 100 pixels. The measurements yielded the following results were done with the following settings on the cavity dumper and yielded the results that can be seen in Figure 11.

Phase	0.2 ns
Division ratio	—
Power (of the RF signal)	13.5 W
Pulse width	11.1 ns
Pulse delay	2.2 ns
Trigger mode	extern

Table 1: The settings on the cavity dumper during measurements.

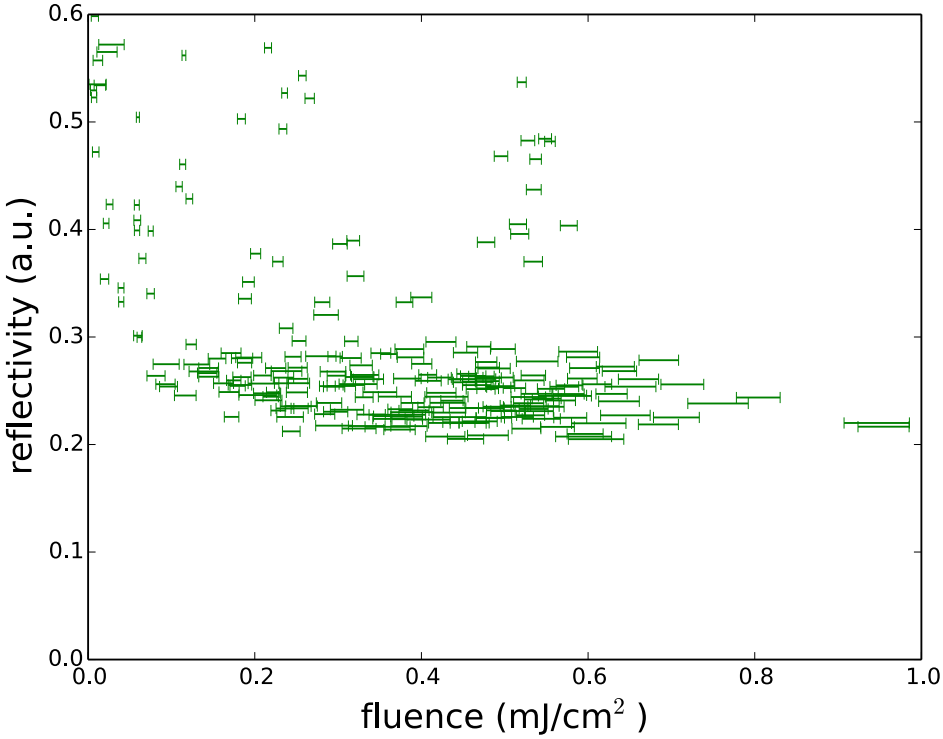

Figure 11: The reflectivity in arbitrary units plotted against the fluence. Most of the data seems to be around a value of 0.25 for reflectivity.

From the figure, there seems to be no relation between the power and the reflectivity. Most points have roughly the same reflectivity (0.25). However, the way data was processed is flawed. For fitting, we assumed a spot that was shaped as a Gaussian. But when we look at the data, this does not seem to be the case. Fitting a Gaussian to something else gives inaccurate results for spotsize and thus fluence. The spotsize fluctuates, which distorts the data for the fluence. In Figure 12 we see what the spot looks like.

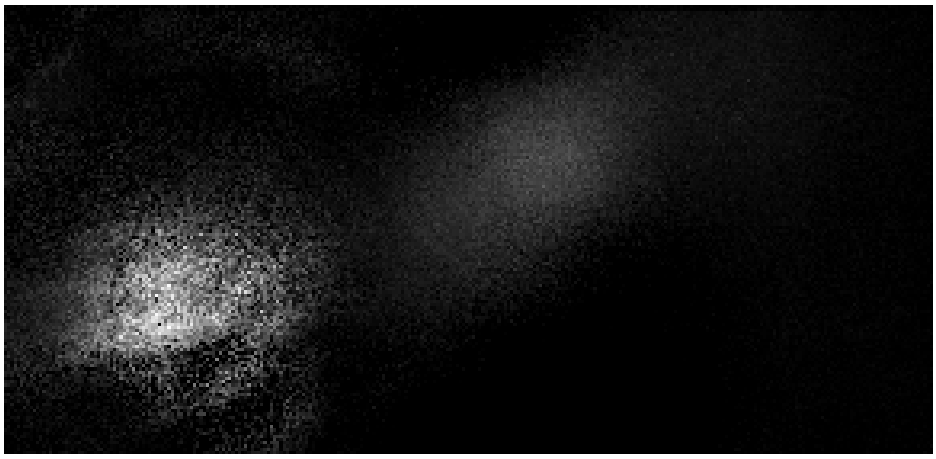

Figure 12: The spot as seen on the camera. The spot on the left is the reference beam, the spot on the right is the beam reflected by the sample.

To work around this, we have chosen to take a fixed spotsize. By looking at the data we determined that most of the shots had a width of around 40 pixels. We chose a fixed spotsize of a square with sides of 40 pixels, corresponding with 2.6 μm. The reflectivity is still taken as the ratio of the pixel sum of the reflected beam and the reference beam. No further selection was made, so all the data points are included in this approach. Figure13 shows the reflectivity plotted against the fluence. Because the reference beam is not subjected to random fluctuations caused by the vibrations of the surface, it has a more or less constant value. This causes data points that have a low intensity of the reflected beam to give a abnormally high value for reflectivity. The uncertainties are based on a Poisson distribution of the data. The ratio of the intensities in arbitrary units (vertical axis in Fig 11) have been scaled to match the normal dimensionless unit of reflectivity. A linear fit to the data gives us a value for the reflectivity of 0.0201 ± 0.0001.

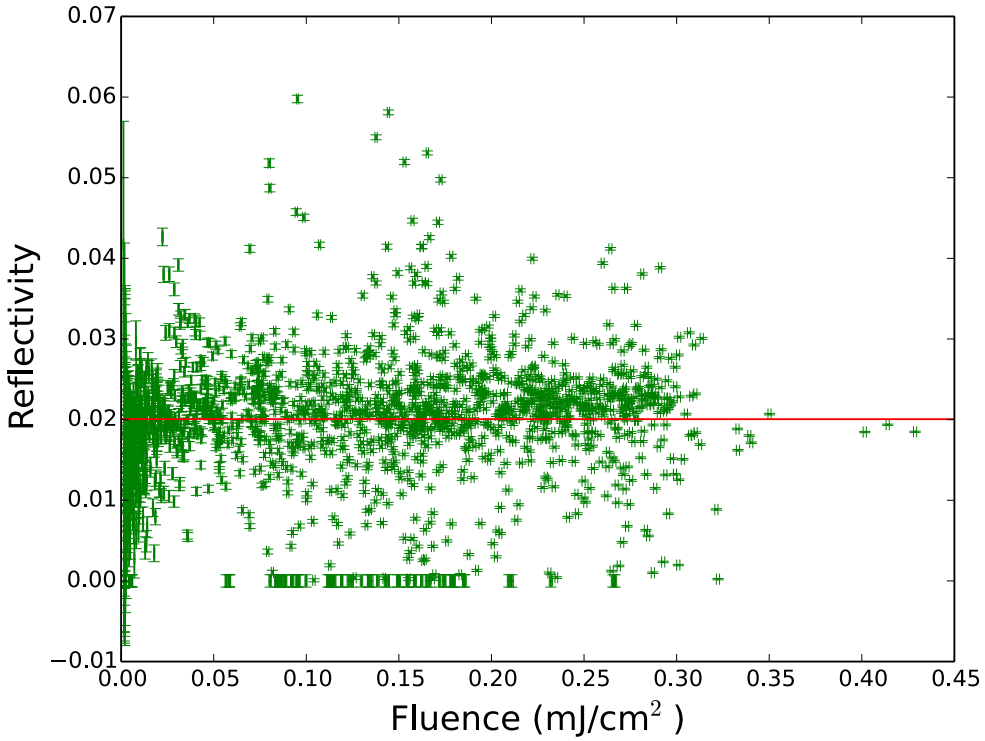

Figure 13: The reflectivity plotted against the fluence with a fixed spotsize. Again, the reflectivity seems to be spread around a constant value. The read line is a scaled linear fit to the data and gives a value of 0.0201 ± 0.0001 for the reflectivity.

The data from Figures 11 and 13 show us that we never reached ablation threshold, meaning we measured the normal reflectivity of the surface instead of the changed reflectivity caused by the plasma. The maximum fluence is in the mJ/cm^2 while we should be in the J/cm^{2}range. This is a problem caused by the laser or the cavity dumper. By placing a power meter directly behind the output of the laser, we found that the laser is only delivering 1 nJ per pulse, while this should be >60nJ (from the data sheet). This is likely to be caused by misalignment in the laser. As the laser has only just been installed, the supplier has been contacted to service the laser.
Another problem during the measurements are waves on the water surface caused by vibrations in the optical table. The objective has a very small depth of focus ($\sim 1\mu m$) so a surface wave of amplitude 0.5 μm causes the surface to be out of focus at the crests and troughs. When focusing with the lamp, this problem was not so apparent. The lamp illuminates a larger area than the the

laser, making it less sensitive to the waves. However, when the laser is used, the waves become a problem. Figure 14 shows two consecutive measurements to illustrate much of a problem the waves are. The reference shot has to be done at the same focus as the normal shots, so the time-dependence of the focus renders the reference shots useless.

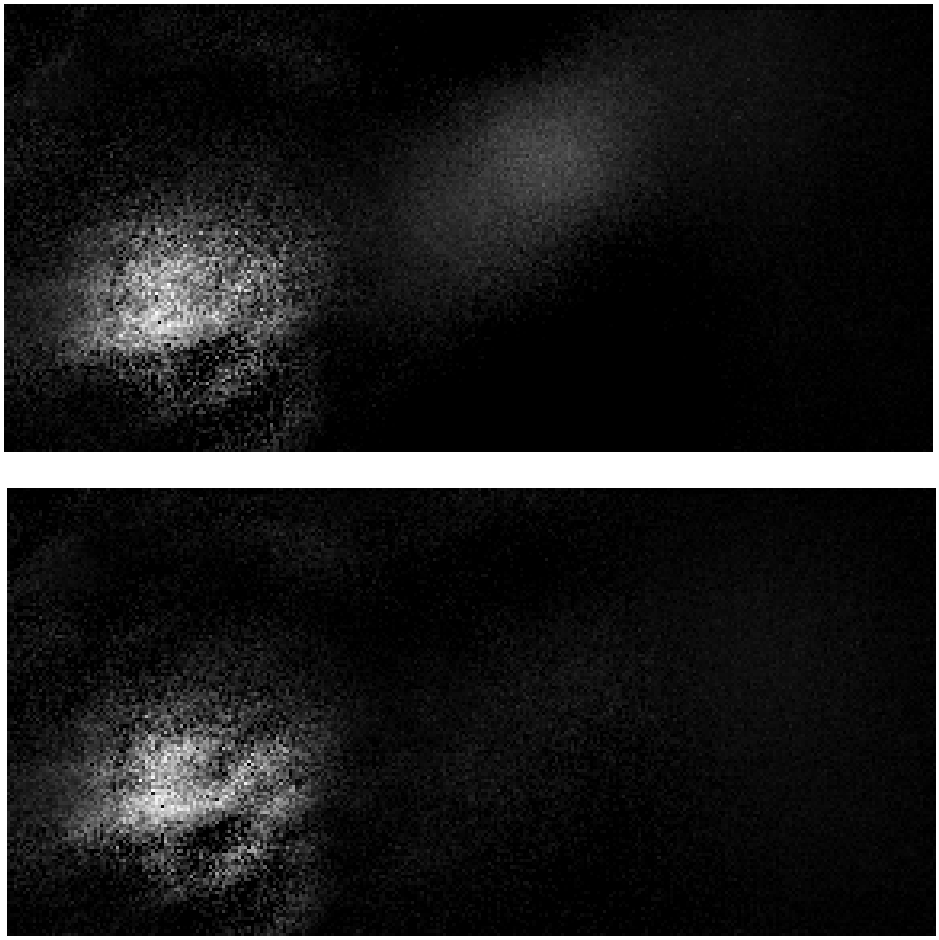

Figure 14: Two consecutive measurements. The time difference between these two shots is 0.6 ms. The top figure shows a spot on the right side (the reflected beam). The bottom figure shows only the reference beam. The reflected spot is defocused so much that it has disappeared completely. The second data point is omitted by the criteria of the first processing method. In the second method it is included resulting in a point with a very low reflectivity.

This problem can be solved by implementing active dampening in the optical table. It can also be by manually selecting the data points that do have a spot.

This process can be automated, but the restrictions have to be selected very carefully, or else it will result in distorted data like in Figure 11. Lowering the exposure time of the camera and increasing the pulse contrast will raise the signal to background ratio. With a high enough signal to background ratio, reference shots would not be necessary, avoiding the problem of the different foci.
This data can be used for calibration of the reflectivity of a water surface. Above ablation threshold, we are looking for a change in the reflectivity and not necessarily the reflectivity itself. To notice a change in reflectivity, one must know what the reflectivity was in the first place. The data from both methods show enough similarities to see that the unchanged reflectivity of a water surface is 0.262 ± 0.02.. To see a significant change in reflectivity, one must reach fluence to structurally exceed a value of 0.36 in reflectivity.

5 Conclusion & discussion

We did not succeed in measuring the change in reflectivity of a water surface under ablation conditions. The technical difficulties have to be solved first. The laser needs to be optimized by an expert, and something needs to be done about the vibrating optical table.
After building the setup we solved some aspects of the technical difficulties. Most of the leakage was cut off by spatial filtering and by applying selective criteria on the data we managed to omit part of the vibration related problems. Increasing pulse contrast and lowering exposure time could also solve the problems caused by the vibrations. We did manage to measure the normal reflectivity of a water surface, which can be used in further experiments when the setup is optimized. This reflectivity was measured to be 0.0201 ± 0.0001

6 Acknowledgements

I would like to thank everyone at the nanophotonics group for giving me such a pleasant time during my research. It definitely changed my view of experimentalists. First of all, I would like to thank Marcel Scholten. Without him, this thesis would be only a few pages. I would also like to thank him for the ego boost he gave me by losing so many matches of ping pong to me. I would like to thank Dries van Oosten for his supervising and advice. We will see each other on stage next year. Thank you, Gordian Zomer for helping with all the computer related problems, and for being a worthy opponent at the ping pong table. Thank you Ole Mussmann for letting me use your simulation software. Thank you, Cees de Kok for trying to fix the laser. Thanks to Dante Killian for creating the extra pieces of electronics we needed. I would like to thank Paul Jurrius for the pieces of hardware he made, and for the great stunts he performed at the barbecue. Thanks go out to James Findley de Regt and Robbert Schoo opening my eyes about bacon on a tosti and for distracting me with the same song for two days straight and thanks to Sebastiaan Greveling for keeping our lab tidy and for making fun of Marcel. I would like to conclude this thesis with a quote from my all time favourite band Foo Fighters: "DONE I'M DONE AND I'M ONTO THE NEXT!"

References

[1] S. E. Black. Laser ablation: Effects and applications, 2011.

[2] Samuel s. Mao. Laser ablation fundamentals & applications, 2015.

[3] S. M. Nikiforov, S. S. Alimpiev, M. W. George, B. G. Sartakov, and Y. O. Simanovsky. Anomalous reflection of water surface during laser ablation. *Optics Communications*, 182(1-3):17–24, 2000. Cited By :4.

[4] Y. Utsunomiya, T. Kajiwara, T. Nishiyama, K. Nagayama, S. Kubota, and M. Nakahara. Laser ablation of liquid surface in air induced by laser irradiation through liquid medium. *Applied Physics A: Materials Science and Processing*, 101(1):137–141, 2010. Cited By :1.

[5] University of stuttgart. Acousto-optic deflector (aod).

[6] Coherent. Mira 900 laser operator's manual.

[7] Young & Freedman. *University Physics With Modern Physics*. 2008.

[8] A.P.E. Angewandte Physik & Elektronik GmbH. *PulseSwitch Cavity Dumper User Manual*. 2013.

[9] E. J. Hemsworth. Laser-induced plasmas: Theory and applications, 2013.

[10] J. R. Hook and H. E. hall. *Solid State Physics*. 2010.

[11] H. Zhang. Single-shot femtosecond laser ablation on the nanoscale, 2013.